Fluid Dynamics & Materials Processing

Tech Science Press

DOI: 10.32604/fdmp.2022.019796

ARTICLE

Influence of Thermophoresis and Brownian Motion of Nanoparticles on Radiative Chemically-Reacting MHD Hiemenz Flow over a Nonlinear Stretching Sheet with Heat Generation

S. Mohammed Ibrahim[1], P. Vijaya Kumar[2] and G. Lorenzini[3,*]

[1]Department of Engineering Mathematics, College of Engineering, Koneru Lakshmaiah Education Foundation, Vaddeswaram, Andhra Pradesh, 522302, India

[2]Department of Mathematics, GITAM (Deemed to be University), Visakhapatnam, Andhra Pradesh, 530045, India

[3]Department of Industrial Engineering, University of Parma-Parco Area Delle Scienze , Parma, 43124, Italy

[*]Corresponding Author: G. Lorenzini. Email: giulio.lorenzini@unipr.it

Received: 15 October 2021 Accepted: 22 February 2022

ABSTRACT

In this study, a radiative MHD stagnation point flow over a nonlinear stretching sheet incorporating thermophoresis and Brownian motion is considered. Using a similarity method to reshape the underlying Partial differential equations into a set of ordinary differential equations (ODEs), the implications of heat generation, and chemical reaction on the flow field are described in detail. Moreover a Homotopy analysis method (HAM) is used to interpret the related mechanisms. It is found that an increase in the magnetic and velocity exponent parameters can damp the fluid velocity, while thermophoresis and Brownian motion promote specific thermal effects. The results also demonstrate that as the Brownian motion parameter is increased, the concentration values become smaller.

KEYWORDS

Hiemenz flow; MHD; thermal radiation; nonlinear stretching; chemical reaction; HAM

1 Introduction

Nanofluids are nanometer-sized particles less than 100 nanometres in size that are introduced into base fluids such as oil, water, bio fluids, ethylene, and lubricants. Despite their essential worth in industry, medicine, and a variety of other efficacious domains of science and technology, countless researchers have gained an interest in nanofluids as opposed to other fluids. However, nanofluids still occupy an indispensable key position in medical sectors, such as the use of gold nanoparticles in the screening of cancerous tumours and the processing of minuscule bombs that are exploited to eradicate cancerous tumours. Choi [1] was the one who came up with the idea of nano materials. He inferred from his observations that infusing these particles strengthens the thermal conductivity of the fluid. Hayat et al. [2] produced analytical solutions for MHD nanofluid squeezing flow between two parallel plates. Hussain et al. [3] studied the dynamics of Jeffery nano-fluid across an exponentially stretched sheet, but also radiation consequences. In a magnetised nanofluid flow, Abbas et al. [4] investigated the role of thermal radiation and chemical reaction response. Hayat et al. [5] studied the characteristics of heat and mass transfer by imposing the convective conditions. Ganesh Kumar et al. [6] have investigated the boundary

layer flows and melting heat transfer of a Prandtl fluid over a stretching surface in the presence of fluid particle suspensions. Jalali et al. [7] conducted a numerical investigation of the competition between viscosity and thermal conductivity about their effects on heat transfer by Al_2O_3-water nanofluid. Much insight on this theme can be found in [8–12].

Modern metallurgical and metal-working technologies rely heavily on understanding MHD flow of an electrically-conducting fluid. Mabood et al. [13] acknowledged the Laplace transform outcomes for the unsteady natural convective motion of revolving magnetohydrodynamics motion in a permeable medium over an oscillating sheet. Mahantesh et al. [14] inspected the effect of the chemical reaction of a magnetohydrodynamic free convective motion of a moving liquid over a vertical sheet. The problem of Marangoni mixed convection in the presence of an inclined magnetic field with uniform strength in a nanofluid is addressed numerically by Sastry et al. [15].

The Hiemenz flow pattern, including its applications in the monitoring of flows over submarine tips, ship tips, and aeroplanes, occupies a crucial role in the exploration of many industrial and natural phenomena. It's also essential in various of fields, including hydrodynamic processes, electronic fan cooling, and nuclear device freezing, to name a few. The optimum values to the aforementioned phenomenon were provided by Ariel [16]. Motsa et al. [17] ascertained numerically the Maxwell fluid outcomes for two-dimensional Hiemenz flow on the way to a diminishing sheet. Parand et al. [18] assessed Hiemenz flow with heat transfer through a porous medium of an incompressible non-Newtonian Rivlin-Ericksen fluid.

In many industries, the significance of thermal radiation on MHD flow and heat transfer is rapidly getting crucial. Heat transfer by thermal radiation has substantial applications in space technology and projects that grasps high temperatures. Aamir Hamid et al. [19] looked at the implications of variable thermal conductivity on MHD Williamson nanofluid flow. A porous mechanism is a material that has a solid matrix and has an interconnected void that allows fluid to flow through it. Pandey et al. [20] reported the collective impact of thermal radiation and porous medium nanofluid flow. Bandari [21] examined the steady state of the two-dimensional incompressible magnetohydrodynamics (MHD) flow of a micropolar nanofluid over a stretching sheet in the presence of chemical reactions, radiation and viscous dissipation. Inayat et al. [22] examined the two-dimensional nanomaterials based mixed flow. The consequences of thermal radiation on convective phenomena in MHD nanofluid over a non-linear stretching surface under heat generation and chemical reaction were studied by considering thermophoresis and Brownian motion using HAM [23–27].

In evident references to modern works, our investigation "The effects of thermal radiation and chemical reaction on MHD Hiemenz flow over a non-linear stretching sheet in presence of thermophoresis and Brownian motion" will certainly appear more viable now. The investigation is approved out for the 2D steady MHD Hiemenz flow. Using a similarity method to reshape the underlying Partial differential equations into a set of ordinary differential equations (ODEs), the implications of heat generation, and chemical reaction on the flow field are described in detail. Moreover a Homotopy analysis method (HAM) is used to interpret the related mechanisms. The influence of numerous parameters is graphically studied and numerically investigated.

2 Mathematical Formulation

We review a non-linear continuously stretched horizontal plate impinging on a steady, two-dimensional, incompressible stagnation-point flow. The plate and free stream velocities are analogous to x^m, while the magnetic field and mass transfer velocity are analogous to $x^{(m-1)/2}$, where x is the distance around the plate from the plate's leading edge. Fig. 1 describes the flow model. The relevant interpretations have been developed in this study:

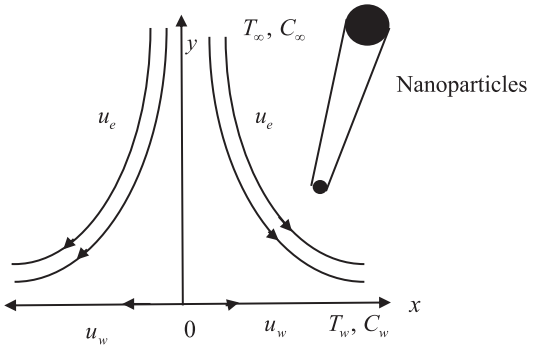

Figure 1: Physical model of the flow

- x and y axes are taken as the way of sheet motion and normal to the motion.
- The nonlinear stretching velocity of the flat plate is assumed as $\bar{u}_w(\bar{x}) = u_0\left(\frac{\bar{x}}{l}\right)^m$, where u_0 is a constant indicates the direction of the plate along positive or negative side of the x axis depending on $u_0 > 0$ or $u_0 < 0$ and a stationary plate when $u_0 = 0$, m is the power-law velocity exponent, l is the characteristic length.
- The ambient fluid's moving velocity has the form $\bar{u}_e(\bar{x}) = u_\infty\left(\frac{\bar{x}}{l}\right)^m$, where u_∞ is a constant.
- A variable magnetic field $B(\bar{x}) = B_0\left(\frac{\bar{x}}{l}\right)^{\frac{m-1}{2}}$, where B_0 is a constant is assumed along the plate.

Under above assumptions, the governing equations are

$$\frac{\partial \bar{u}}{\partial \bar{x}} + \frac{\partial \bar{v}}{\partial \bar{y}} = 0, \tag{1}$$

$$\bar{u}\frac{\partial \bar{u}}{\partial \bar{x}} + \bar{v}\frac{\partial \bar{u}}{\partial \bar{y}} = \bar{u}_e\frac{d\bar{u}_e}{d\bar{x}} + \nu\frac{\partial^2 \bar{u}}{\partial \bar{y}^2} - \frac{\sigma B^2(\bar{x})}{\rho}(\bar{u} - \bar{u}_e), \tag{2}$$

$$\bar{u}\frac{\partial T}{\partial \bar{x}} + \bar{v}\frac{\partial T}{\partial \bar{y}} = \alpha\frac{\partial^2 T}{\partial \bar{y}^2} - \frac{1}{\rho C_p}\frac{\partial q_r}{\partial \bar{y}} + \tau\left(\frac{D_T}{T_\infty}\left(\frac{\partial T}{\partial \bar{y}}\right)^2 + D_B\frac{\partial T}{\partial \bar{y}}\frac{\partial C}{\partial \bar{y}}\right) + \frac{Q_0}{\rho C_p}(T - T_\infty), \tag{3}$$

$$\bar{u}\frac{\partial C}{\partial \bar{x}} + \nu\frac{\partial C}{\partial \bar{y}} = D_B\left(\frac{\partial^2 C}{\partial \bar{y}^2}\right) + \frac{D_T}{T_\infty}\left(\frac{\partial^2 T}{\partial \bar{y}^2}\right) - k_0(C - C_\infty). \tag{4}$$

where $\bar{u}$, $\bar{v}$ are respectively the velocity constituents on the way to the $\bar{x}$ and $\bar{y}$ directions, σ is the electrical conductivity of the fluid, ρ is the fluid density, τ is the ratio of heat capacity of nanoparticles to the base fluid, D_T is the thermophoretic diffusion coefficient, D_B is the Brownian diffusion coefficient, $\alpha = \frac{k}{\rho C_p}$ is the thermal diffusivity, k is the thermal conductivity, T is the fluid temperature, C is the fluid concentration, C_p is the specific heat at constant pressure, T_∞ and C_∞ are the ambient temperature and concentration of the fluid, k_0 is the dimensional chemical reaction, Q_0 is the heat source coefficient.

The appropriate boundary conditions are

$$\begin{aligned} &\bar{u} = \bar{u}_w(\bar{x}), \quad \bar{v} = 0, \quad T = T_w, \quad C = C_w \quad \text{at} \quad \bar{y} = 0 \\ &u = \bar{u}_e(\bar{x}), \qquad\qquad T = T_\infty, \quad C = C_\infty \quad \text{as} \quad \bar{y} \to \infty, \end{aligned} \tag{5}$$

where $\bar{u}_e(\bar{x})$ is the potential velocity, $\overline{u}_w(\bar{x})$ is the velocity of the plate, T_w and C_w are the plate temperature and plate concentration.

The radiative heat flux is determined by using Rosseland approximation

$$q_r = \frac{4\sigma^*}{3k^*}\frac{\partial T^4}{\partial y},$$

where σ^* is the Stefan-Boltzman constant and k^* is the mean absorption coefficient. We recognise that the disparity in temperature within the flow makes sure that in a Taylor's sequence, T4 can be extended. Hence, established T^4 in Taylor series about T_∞, we obtain $T^4 = 4T_\infty^3 T - 3T_\infty^4$.

Now, we introduce the following similarity transformations:

$$\begin{gathered} x = \frac{\overline{x}}{l},\ \ y = \frac{\overline{y}\sqrt{\mathrm{Re}}}{l},\ \ u = \frac{\overline{u}}{u_\infty},\ v = \frac{\overline{v}\sqrt{\mathrm{Re}}}{u_\infty},\ \ u_e = \frac{\overline{u}_e}{u_\infty},\ \ \zeta = \frac{\overline{y}\sqrt{\mathrm{Re}}}{l}x^{\frac{1-m}{2}},\ \ \theta = \frac{T-T_\infty}{T_w-T_\infty}, \\ \phi = \frac{C-C_\infty}{C_w-C_\infty},\ \ \psi = x^{\frac{m+1}{2}}f(\zeta),\ \ u = x^m f'(\zeta),\ \ v = -\left[\frac{m+1}{2}x^{\frac{m-1}{2}}f(\zeta) + \frac{m-1}{2}yx^{m-1}f'(\zeta)\right] \end{gathered} \tag{6}$$

Substituting Eq. (6) in Eqs. (2)–(5), we obtain

$$f''' + \frac{m+1}{2}ff'' + m(1-f'^2) + M(1-f') = 0, \tag{7}$$

$$\frac{1}{\mathrm{Pr}}\left(1+\frac{4}{3}R\right)\theta'' + \frac{m+1}{2}f\,\theta' + Nb\theta'\phi' + Nt\theta'^2 + Q\,\theta = 0, \tag{8}$$

$$\phi'' + \frac{m+1}{2}Lef\,\phi' + \frac{Nt}{Nb}\theta'' - Le\,\gamma\,\phi = 0, \tag{9}$$

where $\mathrm{Pr} = \frac{v}{\alpha}$ is the Prandtl number, $M = \frac{\sigma B_0^2 l}{\rho u_\infty}$ is the magnetic parameter, $R = \frac{4\,\sigma^*\,T_\infty^3}{k^* k}$ is the radiation parameter, $Nb = \frac{\tau D_B(T_w - T_\infty)}{v}$ is the Brownian motion parameter, $Nt = \frac{\tau D_T(C_w - C_\infty)}{T_\infty v}$ is the thermophoresis parameter, $Q = \frac{Q_0}{\rho C_p u_\infty x^{m-1}}$ is the heat generation/absorption parameter, $Le = \frac{v}{D_B}$ is the Lewis number, $\gamma = \frac{k_0}{u_\infty x^{m-1}}$ is the chemical reaction parameter.

The boundary conditions are

$$\begin{gathered} f = 0,\quad f' = V,\quad \theta = 1,\quad \phi = 1 \quad \text{at} \quad \zeta = 0, \\ f' = 1,\quad \theta = 0,\quad \phi = 0 \quad \text{as} \ \ \zeta \to \infty, \end{gathered} \tag{10}$$

where prime denotes differentiation with respect to ζ, $V = \frac{u_0}{u_\infty}$ is the velocity ratio parameter, $V > 0$ reflects that the plate is progressing in the identical manner as the free stream velocity, $V < 0$, implies that the plate is heading in the contrary side of the free stream and $V = 0$ stands for static plate. The case $0 < V < 1$ designates that the plate's mobility is slower than that of the free-flowing fluid and $V > 1$ designates the mobility is greater. $V = 1$ is the case When the plate and the fluid proceed at the same velocity.

Non-dimensional skin friction coefficient C_f and Nusselt number Nu_x are

$C_{f\bar{x}} = \dfrac{2\tau_w}{\rho \bar{u}_e^2}$, where $\tau_w = \mu(\nabla \bar{u})_{\bar{y}=0}$, $Nu_{\bar{x}} = \dfrac{\bar{x} q_w}{k(T_w - T_\infty)}$ and the Sherwood number $Sh_{\bar{x}} = \dfrac{\bar{x} q_m}{D_B(C_w - C_\infty)}$,

where q_w and q_m are the heat flux and mass flux at the surface respectively given by

$$q_w = \left(-\left(k + \frac{16\sigma^* T_\infty^3}{3k^*} \right) (\nabla T) \right)_{\bar{y}=0}, \quad q_m = -(D_B(\nabla C))_{\bar{y}=0}$$

Substituting q_w and q_m in the preceding equation, we get

$$C_f = C_{f\bar{x}} \mathrm{Re}_{\bar{x}}^{1/2} = f''(0), \quad Nu = \mathrm{Re}_x^{-1/2} Nu_{\bar{x}} = -\left(1 + \frac{4}{3}R\right)\theta'(0) \text{ and } Sh = Sh_x (\mathrm{Re}_{\bar{x}})^{-1/2} = -\phi'(0)$$

where $\mathrm{Re}_{\bar{x}} = \dfrac{\bar{u}_e \bar{x}}{\nu}$ is the local Reynolds number.

3 Solution Methodology

3.1 HAM

We now adopt aforementioned initial guesses and linear operators to encapsulate the homotopic solutions of Eqs. (7)–(10):

$$f_0(\zeta) = \zeta + (V-1)(1 - e^{-\zeta}),$$
$$\theta_0(\zeta) = e^{-\zeta},$$
$$\phi_0(\zeta) = e^{-\zeta},$$

$$L_1(f) = f''' - f',$$
$$L_2(\theta) = \theta'' - \theta,$$
$$L_3(\phi) = \phi'' - \phi,$$

with

$$L_1\left(C_1 + C_2 e^{\zeta} + C_3 e^{-\zeta}\right) = 0,$$
$$L_2\left(C_4 e^{\zeta} + C_5 e^{-\zeta}\right) = 0,$$
$$L_3\left(C_6 e^{\zeta} + C_7 e^{-\zeta}\right) = 0,$$

where $C_i\,(i = 1 \text{ to } 7)$ are the arbitrary constants.

We construct the zeroth-order deformation equations

$$(1-p)\,L_1(f(\zeta;\ p) - f_0(\zeta)) = p\,\hbar_1\,N_1[f(\zeta;\ p)]\,, \tag{11}$$

$$(1-p)\,L_2(\theta(\zeta;\ p) - \theta_0(\zeta)) = p\,\hbar_2\,N_2[f(\zeta;\ p),\ \theta(\zeta;\ p),\ \phi(\zeta;\ p)]\,, \tag{12}$$

$$(1-p)\,L_3(\phi(\zeta;\ p) - \phi_0(\zeta)) = p\,\hbar_3\,N_3[f(\zeta;\ p),\ \theta(\zeta;\ p),\ \phi(\zeta;\ p)], \tag{13}$$

subject to the boundary conditions

$$\begin{aligned} &f(0;\ p) = 0, \quad f'(0;\ p) = V, \quad f'(\infty;\ p) = 1, \\ &\theta(0;\ p) = 1, \qquad\qquad\quad \theta(\infty;\ p) = 0, \\ &\phi(0;\ p) = 1, \qquad\qquad\quad \phi(\infty;\ p) = 0, \end{aligned} \tag{14}$$

where

$$N_1[f(\zeta;\ p)] = \frac{\partial^3 f(\zeta;\ p)}{\partial \zeta^3} + \frac{m+1}{2} f(\zeta;\ p) \frac{\partial^2 f(\zeta;\ p)}{\partial \zeta^2} + m\left(1 - \left(\frac{\partial f(\zeta;\ p)}{\partial \zeta}\right)^2\right) + M\left(1 - \frac{\partial f(\zeta;\ p)}{\partial \zeta}\right), \tag{15}$$

$$N_2[f(\zeta;\ p),\ \theta(\zeta;\ p),\ \phi(\zeta;\ p)] = \frac{1}{\mathrm{Pr}}\left(1 + \frac{4}{3}R\right)\frac{\partial^2 \theta(\zeta;\ p)}{\partial \zeta^2} + \frac{m+1}{2}\left(f(\zeta;\ p)\ \frac{\partial \theta(\zeta;\ p)}{\partial \zeta}\right) + Nb \frac{\partial \theta(\zeta;\ p)}{\partial \zeta}\frac{\partial \phi(\zeta;\ p)}{\partial \zeta} + Nt\left(\frac{\partial \theta(\zeta;\ p)}{\partial \zeta}\right)^2 + Q\,\theta(\zeta;\ p), \tag{16}$$

$$N_3[f(\zeta;\ p),\ \theta(\zeta;\ p),\ \phi(\zeta;\ p)] = \frac{\partial^2 \phi(\zeta;\ p)}{\partial \zeta^2} + \frac{m+1}{2} Le f(\zeta;\ p)\ \frac{\partial \phi(\zeta;\ p)}{\partial \zeta} + \frac{Nt}{Nb}\frac{\partial^2 \theta(\zeta;\ p)}{\partial \zeta^2} - Le\,\gamma \phi(\zeta;\ p), \tag{17}$$

where $p \in [0,\ 1]$ is the embedding parameter, $\hbar_1$, $\hbar_2$ and $\hbar_3$ are non-zero auxiliary parameters and N_1, N_2 and N_3 are nonlinear operators.

The nth-order deformation equations are follows:

$$L_1(f_n(\zeta) - \chi_n f_{n-1}(\zeta)) = \hbar_1 R_n^f(\zeta), \tag{18}$$

$$L_2(\theta_n(\zeta) - \chi_n\,\theta_{n-1}(\zeta)) = \hbar_2 R_n^\theta(\zeta), \tag{19}$$

$$L_3(\phi_n(\zeta) - \chi_n\,\phi_{n-1}(\zeta)) = \hbar_3 R_n^\phi(\zeta), \tag{20}$$

with the following boundary conditions:

$$\begin{aligned} &f_n(0) = 0, \quad f_n'(0) = 0, \quad f_n'(\infty) = 0,\\ &\theta_n(0) = 0, \qquad\qquad \theta_n(\infty) = 0,\\ &\phi_n(0) = 0, \qquad\qquad \phi_n(\infty) = 0, \end{aligned} \tag{21}$$

where

$$R_n^f(\zeta) = f_{m-1}^{'''} + \frac{m+1}{2}\sum_{i=0}^{m-1} f_{m-1-i} f_i^{''} - m\sum_{i=0}^{m-1} f'_{m-1-i} f_i^{'} + (1-\chi_m)(m+M) - M f_{m-1}^{'}, \tag{22}$$

$$R_n^\theta(\zeta) = \frac{1}{\mathrm{Pr}}\left(1 + \frac{4R}{3}\right)\theta_{n-1}^{''} + \frac{m+1}{2}\sum_{i=0}^{n-1} f_{n-1-i}\,\theta_i^{'} + Nb\sum_{i=0}^{n-1}\theta'_{n-1-i}\,\phi_i^{'} + Nt\sum_{i=0}^{n-1}\theta'_{n-1-i}\,\theta_i^{'} + Q\,\theta_{n-1}, \tag{23}$$

$$R_n^\phi(\zeta) = \phi''_{n-1} + Le\left(\frac{m+1}{2}\sum_{i=0}^{n-1} f_{n-1-i}\,\phi'_i - \gamma\phi_{m-1}\right) + \frac{Nt}{Nb}\theta''_{m-1}, \tag{24}$$

$$\chi_n = \begin{cases} 0, & n \le 1,\\ 1, & n > 1. \end{cases}$$

Here we choose $H_1(\zeta) = H_2(\zeta) = H_3(\zeta) = e^{-\zeta}$.

3.2 Convergence of HAM Solution

The auxiliary parameters $\hbar_1$, $\hbar_2$ and $\hbar_3$ have a straightforward influence on the convergence and approximation rate of the findings drawn. $\hbar$-curves are interpreted in Fig. 2 in accordance to establish the requisite quantities for both parameters. The principal scenario of the parameters is just about [−2.0, 0.0] as a consequence of such a comprehensive breakdown. For $\hbar_1 = -0.85$, $\hbar_2 = \hbar_3 = -0.65$, in the entire region of ζ, the series solutions are convergent. Table 1 implies the method's convergence.

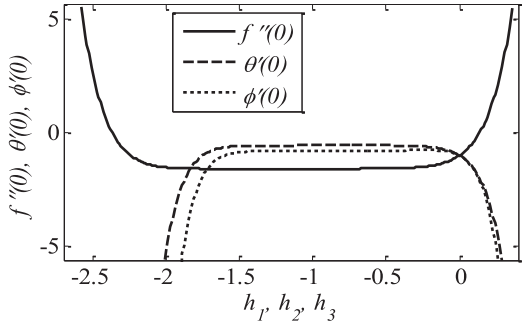

Figure 2: $\hbar$-curves for $f''(0)$, $\theta'(0)$ and $\phi'(0)$ at 15th order approximations

Table 1: Convergence of HAM solution for different orders of approximations when $M = m = 0.5$, $V = 2.0$, $Nb = 0.3$, $Nt = 0.2$, $R = Q = 0.1$, Pr = $Le = 1.0$, $\gamma = 0.2$

Order	$-f''(0)$	$-\theta'(0)$	$-\phi'(0)$
5	1.571170	0.571187	0.804188
10	1.574507	0.570395	0.805292
15	1.574604	0.570188	0.805307
20	1.574608	0.570168	0.805315
25	1.574608	0.570166	0.805313
30	1.574608	0.570166	0.805313
35	1.574608	0.570166	0.805313
40	1.574608	0.570166	0.805313
45	1.574608	0.570166	0.805313

4 Results and Discussions

For a wide range of physical characteristics, tables and charts are often performed to ascertain and describe the nature of flow, temperature, concentration, skin friction coefficient, and local Nusselt and Sherwood numbers. We check out the following values all across the exploration, apart from renovated quantities as revealed in the tables and charts.

$M = m = 0.5,\ V = 2.0,\ Nb = 0.3,\ Nt = 0.2,\ R = Q = 0.1,\ \text{Pr} = Le = 1.0,\ \gamma = 0.2.$

Figs. 3–5 illustrate the impression of magnetic parameter M on distributions. It is insinuated that as M strengthens the velocity distribution of the fluid degrades. Whenever a magnetic field is imparted to an electrically conducting fluid, the Lorentz force generates, and this energy contradicts the flow pattern,

forcing velocity drawings to deteriorate, while the thermal and solutal boundary layer thickness improves. As the space variable turns away from the boundary surface, modifications in the velocity exponent parameter m restrain the growth of the momentum boundary layer, which reaches zero. The plots of temperature and concentration find similar results. This is shown in Figs. 6–8.

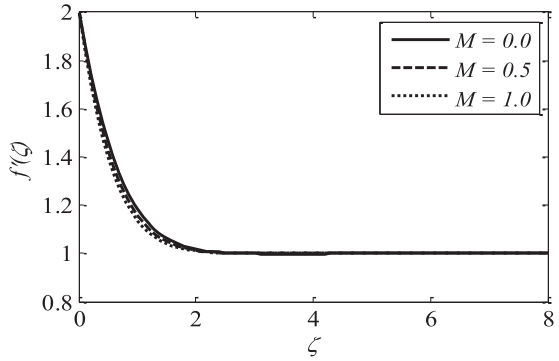

Figure 3: Effect of M on $f'(\zeta)$

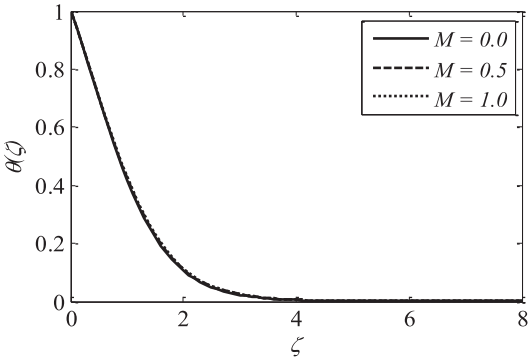

Figure 4: Effect of M on $\theta(\zeta)$

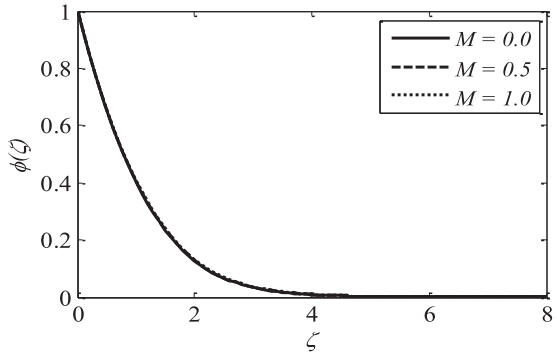

Figure 5: Effect of M on $\phi(\zeta)$

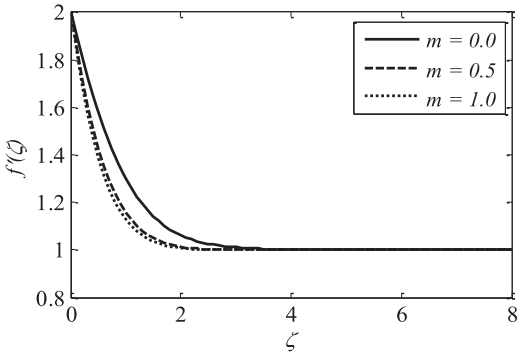

Figure 6: Effect of m on $f'(\zeta)$

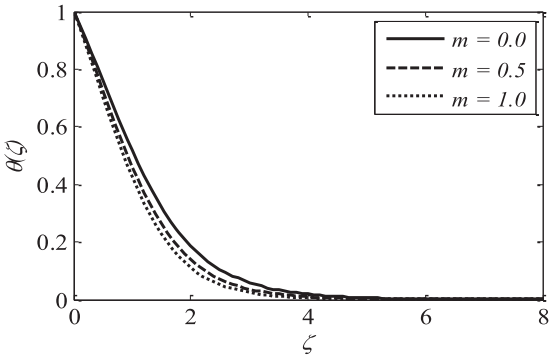

Figure 7: Effect of m on $\theta(\zeta)$

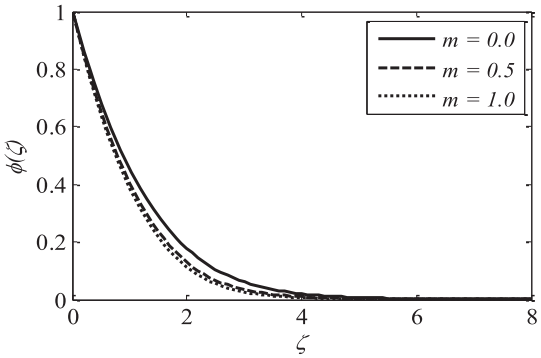

Figure 8: Effect of m on $\phi(\zeta)$

Fluid velocity amplifies as the velocity ratio parameter V accelerates, whereas the fluid temperature and concentration drop. This is observed from Figs. 9–11. Figs. 12 and 13 reveal the implications of the Brownian motion parameter Nb on temperature and concentration fields. Brownian motion, in particular, aids in the heating of the fluid in the boundary layer and the restriction of particle evacuation from the fluid on the surface. As a result, the temperature goes up while the concentration lowers.

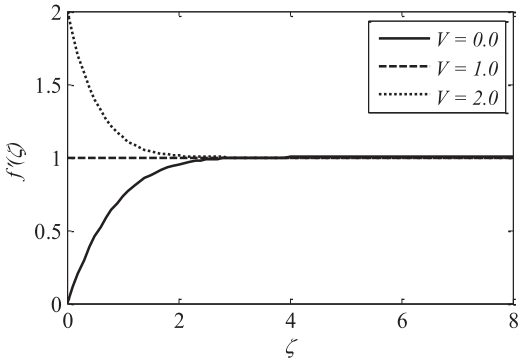

Figure 9: Effect of V on $f'(\zeta)$

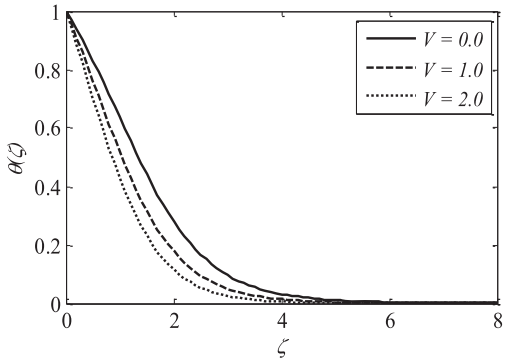

Figure 10: Effect of V on $\theta(\zeta)$

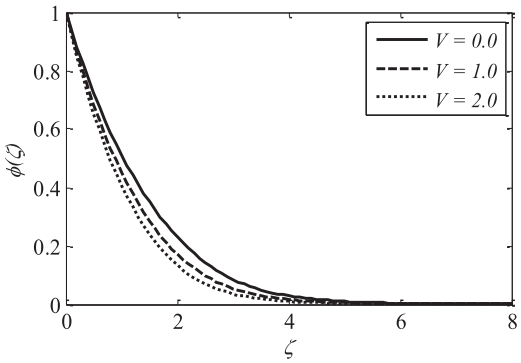

Figure 11: Effect of V on $\phi(\zeta)$

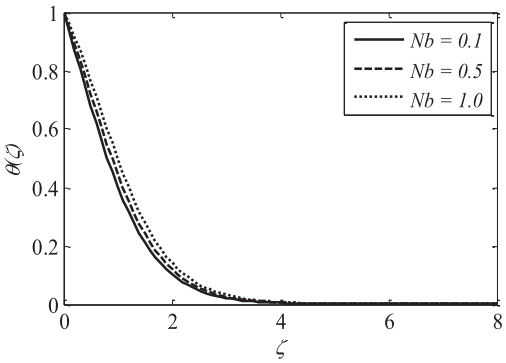

Figure 12: Effect of Nb on $\theta(\zeta)$

The inclusion of nanoparticles externally allowed the thermophoresis parameters Nt to appear. The inclusion of nanoparticles is correlated to the thermal conductivity of liquids. When the amplitude of Nt is improved, the thermal conductivity of the fluid boosts, and this greater thermal conductivity leads to high temperature. We also identified that relatively high Nt values result in greater nanoparticle concentrations. This is shown in Figs. 14 and 15.

Fig. 16 highlights temperature recuperation for diverse levels of the radiation parameter R. With altered measurements of R, temperature sketches accelerate as well. This is owing to the belief that heightened radiative heat transmission makes the establishment of thermal boundary layers simpler. The deviation of Prandtl number Pr on temperature is interpreted in Fig. 17. It is clear from the figure that uplifting values of Pr, temperature accelerates. Heat energy is accomplished in the flow region when the heat source parameter Q is risen, allowing the temperature to rise rapidly. Fig. 18 reflects it.

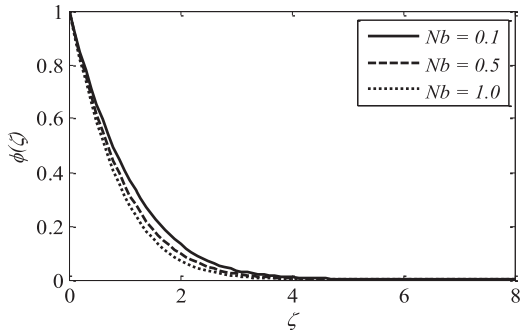

Figure 13: Effect of Nb on $\phi(\zeta)$

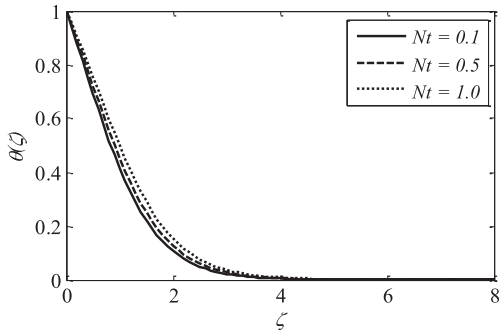

Figure 14: Effect of Nt on $\theta(\zeta)$

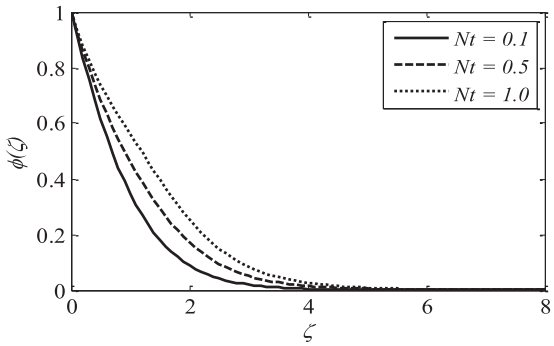

Figure 15: Effect of Nt on $\phi(\zeta)$

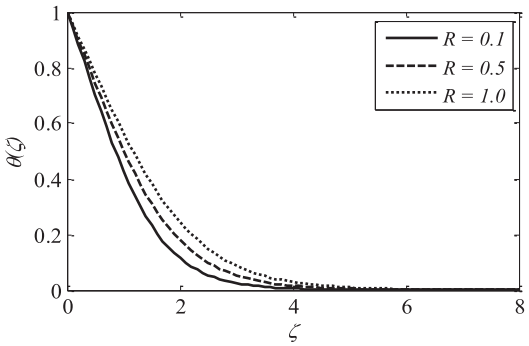

Figure 16: Effect of R on $\theta(\zeta)$

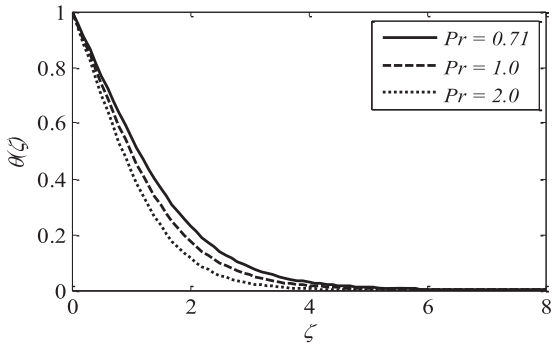

Figure 17: Effect of Pr on $\theta(\zeta)$

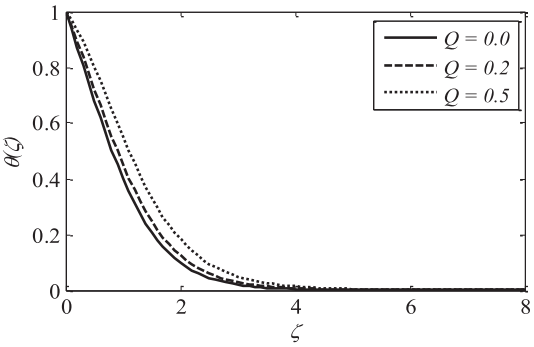

Figure 18: Effect of Q on $\theta(\zeta)$

Fig. 19 illustrates that as the Lewis number Le grows, the concentration distribution of nanoparticles drops. Larger values of Le relate to a poorer Brownian diffusion coefficient, leading in a diminution in the concentration distribution of nanoparticles. The consequence of a chemical reaction parameter on concentration profiles is visualized in Fig. 20. It has been recognised that as the chemical reaction parameter grows, the concentration lowers.

When the plate and fluid advance at the similar tempo $(V = 1)$, the skin friction coefficient is constant (zero). In the scenario of a stationary plate $(V = 0)$, it strengthens with M. When the plate gets faster than the free stream $(V = 2)$, it slows down with M. This is depicted in Fig. 21. Nusselt number amplifies with R and Pr. This is noticed in Fig. 22. From Fig. 23, it is noticed that Sherwood number accelerates with Le and γ.

Assessments of $-f''(0)\ \&\ -\theta'(0)$ with recently existing literature are undertaken in Tables 2 and 3, and the stats indicate a strong and positive correlation.

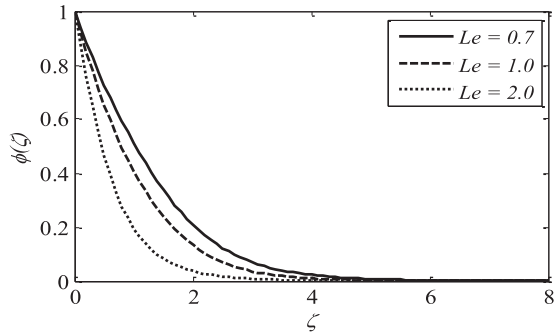

Figure 19: Effect of Le on $\phi(\zeta)$

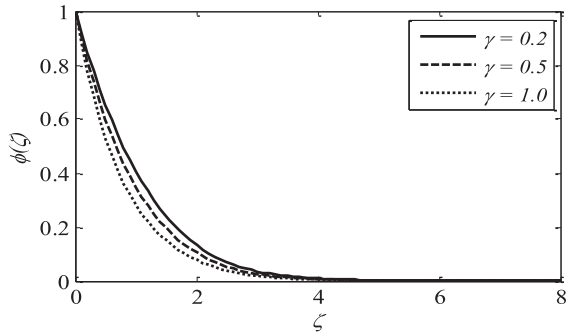

Figure 20: Effect of Nt on $\phi(\zeta)$

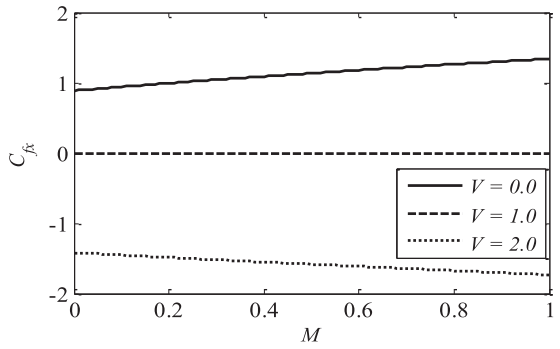

Figure 21: Effect of M and V on C_{fx}

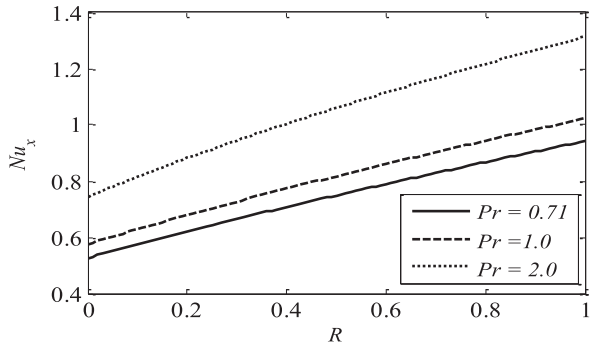

Figure 22: Effect of R and Pr on Nu_x

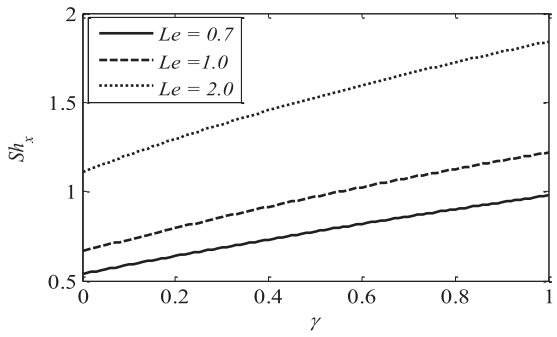

Figure 23: Effect of Le and γ on Sh_x

Table 2: Comparison of $-f''(0)$ when $M = V = 0.0$

m	Uddin et al. [28]	HAM
0.0	0.33206	0.332057
1/3	0.75745	0.757441
1.0	1.23259	1.232587

Table 3: Comparison of $-\theta'(0)$ when $m = 1$, $Nb = Nt = Q = V = 0.0$

M	Kechil et al. [29]	HAM
0.0	0.57035	0.570364
1.0	059539	0.595382

5 Conclusive Remarks

The analytical exploration of two-dimensional steady forced convective flow of a Newtonian fluid past a convectively heated vertically moving plate towards the face of a variable magnetic field and the radiation factor is reviewed in this report using HAM. The foregoing are the crucial insights reached from the graphical and numerical solutions to the problem:

- The temperature profile is significantly amplified by the heat source parameter.
- Thermal radiation and thermophoresis parameters lead enhance temperature.
- The concentration profile lowers as both the Lewis number and the chemical reaction parameters expand.
- The rate of heat transfer elevates with R and Pr.
- The rate of mass transfer elevates with Le and γ.

Acknowledgement: We are very much thankful to learned reviewers for their useful suggestions for the improvement in the quality of our manuscript.

Funding Statement: The authors received no specific funding for this study.

Conflicts of Interest: The authors declare that they have no conflicts of interest to report regarding the present study.

References

1. Choi, S. U. S. (1995). Enhancing thermal conductivity of fluids with nanoparticles. *Proceedings of the ASME International Mechanical Engineering Congress and Exposition, 66,* 99–105.
2. Hayat, T., Sajjad, R., Alsaedi, A., Muhammad, T., Ellahi, R. (2017). On squeezed flow of couple stress nanofluid between two parallel plates. *Results in Physics, 7,* 553–561. DOI 10.1016/j.rinp.2016.12.038.
3. Hussain, T., Shehzad, S. A., Hayat, T., Alsaedi, A., Al-Solamy, F. et al. (2014). Radiative hydromagnetic flow of jeffrey nanofluid by an exponentially stretching sheet. *PLoS One, 9(8),* e103719. DOI 10.1371/journal.pone.0103719.
4. Abbas, M. A., Bhatti, M. M., Sheikholeslami, M. (2019). Peristaltic propulsion of jeffrey nnanofluid with thermal radiation and chemical reaction effects. *Inventions, 4(4),* 68–83. DOI 10.3390/inventions4040068.
5. Hayat, T., Qayyum, S., Alsaedi, A. (2017). Mechanisms of nonlinear convective flow of jeffrey nanofluid due to nonlinear radially stretching sheet with convective conditions and magnetic field. *Results in Physics, 7,* 2341–2351. DOI 10.1016/j.rinp.2017.06.052.
6. Ganesh Kumar, K., Manjunatha, S., Rudraswamy, N. G. (2020). MHD flow and nonlinear thermal radiative heat transfer of dusty prandtl fluid over a stretching sheet. *Fluid Dynamics & Material Processing, 16(2),* 131–146. DOI 10.32604/fdmp.2020.0152.
7. Jalali, H., Abbassi, H. (2020). Analysis of the influence of viscosity and thermal conductivity on heat transfer by Al_2O_3-water nanofluid. *Fluid Dynamics & Materials Processing, 15(3),* 253–270. DOI 10.32604/fdmp.2019.03896.

8. Shamshuddin, M., Krishna, C. B. (2019). Heat absorption and joule heating effects on transient free convective reactive micropolar fluid flow past a vertical porous plate. *Fluid Dynamics & Materials Processing, 15(3),* 207–231. DOI 10.32604/fdmp.2019.00449.
9. Ibrahim, S. M., Lorenzini, G., Kumar, P. V., Raju, C. S. K. (2017). Influence of chemical reaction and heat source on dissipative MHD mixed convection flow of a casson nanofluid over a nonlinear permeable stretching sheet. *International Journal of Heat and Mass Transfer, 111,* 346–355. DOI 10.1016/j.ijheatmasstransfer.2017.03.097.
10. Reddy, T. S., Roja, P., Ibrahim, S. M., Lorenzini, G. (2022). Thermal radiation and viscous dissipation effects on (MHD) bioconvection stream of Maxwell nanoliquid over a permeable vertical plate Due to gyrotactic microorganisms. *Mathematical Modelling of Engineering Problems, 9(2),* 325–335. DOI 10.18280/mmep.090205.
11. Kumar, P. V., Sunitha, Ch., Lorenzini, G., Ibrahim, S. M. (2022). A study of thermally radiant williamson nanofluid over an exponentially elongating sheet with chemical reaction via homotopy analysis method. *CFD Letter, 14(5),* 68–86. DOI 10.37934/cfdl.14.5.6886.
12. Mabood, F., Ibrahim, S. M., Kumar, P. V., Lorenzini, G. (2020). Effects of slip and radiation on convective MHD casson nanofluid flow over a stretching sheet influenced by variable viscosity. *Journal of Engineering Thermophysics, 29,* 303–315. DOI 10.1134/S1810232820020125.
13. Mabood, F., Khan, W. A., Ismail, A. I. M. (2015). MHD boundary layer flow and heat transfer of nanofluids over a nonlinear stretching sheet: A numerical study. *Journal of Magnetism and Magnetic Materials, 374,* 569–576. DOI 10.1016/j.jmmm.2014.09.013.
14. Mahantesh, N., Vajravelu, K., Subhas Abel, M. (2011). Heat transfer in MHD viscoelastic boundary layer flow over a stretching sheet with thermal radiation and non-uniform heat source/sink. *Communications in Nonlinear Science and Numerical Simulation, 16(9),* 3578–3590. DOI 10.1016/j.cnsns.2010.12.033.
15. Sastry, D. R. V. S. R. K., Kameswaran, P. K., Hatami, M. (2021). MHD and viscous dissipation effects in marangoni mixed flow of a nanofluid over an inclined plate in the presence of ohmic heating. *Fluid Dynamics & Materials Processing, 17(2),* 285–300. DOI 10.32604/fdmp.2021.014429.
16. Ariel, P. D. (1994). Hiemenz flow in hydromagnetics. *Acta Mechanica, 103,* 31–43. DOI 10.1007/BF01180216.
17. Motsa, S. S., Khan, Y., Shateyi, S. (2012). A new numerical solution of Maxwell fluid over a shrinking sheet in the region of a stagnation point. *Mathematical Problems in Engineering, 2012,* 290615. DOI 10.1155/2012/290615.
18. Parand, K., Lotfi, Y., Amani Rad, J. (2018). An efficient analytic approach for solving hiemenz flow through a porous medium of a non-newtonian rivlin-ericksen fluid with heat transfer. *Nonlinear Engineering, 7(4),* 287–301. DOI 10.1515/nleng-2017-0160.
19. Aamir Hamid, H., Khan, M. (2018). Unsteady mixed convective flow of williamson nanofluid with heat transfer in the presence of variable thermal conductivity and magnetic field. *Journal of Molecular Liquids, 260,* 436–446. DOI 10.1016/j.molliq.2018.03.079.
20. Pandey, A. K., Kumar, M. (2017). Natural convection and thermal radiation influence on nanofluid flow over a stretching cylinder in a porous medium with viscous dissipation. *Alexandria Engineering Journal, 56(1),* 55–62. DOI 10.1016/j.aej.2016.08.035.
21. Bhandari, A. (2019). Radiation and chemical reaction effects on nanofluid flow over a stretching sheet. *Fluid Dynamics & Materials Processing, 15(5),* 557–582. DOI 10.32604/fdmp.2019.04108.
22. Inayat, U., Iqbal, S., Manzoor, T. (2022). Theoretical investigation of two-dimensional nonlinear radiative thermionics in nano-MHD for solar insolation: A semi-empirical approach. *Computer Modeling in Engineering & Sciences, 130(2),* 751–776. DOI 10.32604/cmes.2022.018665.
23. Liao, S. J. (2011). *Beyond perturbation: Introduction to Homotopy analysis method*. Boca Raton: Chapman and Hall, CRC Press.
24. Kumar, P. V., Ibrahim, S. M., Jyothsna, K. (2019). Numerical modelling on radiative MHD flow of a chemically casson fluid over an exponentially inclined stretching sheet. *Mathematical Modeling of Engineering Problems, 6(4),* 491–501. DOI 10.18280/mmep.060403.

25. Ibrahim, S. M., Kumar, P. V., Makinde, O. D. (2018). Chemical reaction and radiation effects on non-newtonian fluid flow over a stretching sheet with non-uniform thickness and heat source. *Defect and Diffusion Forum, 387,* 319–331. DOI 10.4028/www.scientific.net/DDF.387.319.
26. Hayat, T., Shehzad, S. A., Alsaedi, A. (2012). Soret and dufour effects on magnetohydrodynamic (MHD) flow of casson fluid. *Applied Mathematics and Mechanics, 33,* 1301–1312. DOI 10.1007/s10483-012-1623-6.
27. Kumar, P. V., Ibrahim, S. M., Lorenzini, G. (2021). Investigation of the heat transfer and flow characteristics on hiemenz flow under the influence of heat source and thermal radiation with hydrodynamic–thermal slips effects. *Journal of Mechanical Engineering Research and Developments, 44(9),* 369–383.
28. Uddin, M. J., Khan, W. A., Ismail, A. I. (2013). MHD forced convective laminar boundary layer flow of convectively heated moving vertical plate with radiation and transpiration effect. *PLoS One, 8(5),* e62664. DOI 10.1371/journal.pone.0062664.
29. Kechil, S. A., Hashim, I. (2009). Approximate analytical solution for MHD stagnation-point flow in porous media. *Communications in Nonlinear Science and Numerical Simulation, 14(4),* 1346–1354. DOI 10.1016/j.cnsns.2008.02.007.